Overexpression of fibroblast growth factor 13 ameliorates amyloid-β-induced neuronal damage

Ruo-Meng Li, Lan Xiao, Ting Zhang, Dan Ren, Hong Zhu*

https://doi.org/10.4103/1673-5374.357902

Date of submission: January 17, 2022

Date of decision: August 2, 2022

Date of acceptance: September 6, 2022

Date of web publication: October 11, 2022

From the Contents

Graphical Abstract

Overexpression of fibroblast growth factor 13 (FGF13) ameliorates amyloid-β-induced neuronal damage through activation of the P13K/AKT/GSK-3β axis

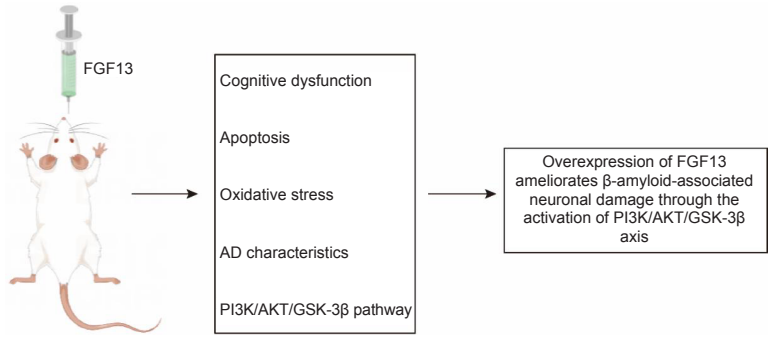

Abstract

Previous studies have shown that fibroblast growth factor 13 is downregulated in the brain of both Alzheimer's disease mouse models and patients, and that it plays a vital role in the learning and memory. However, the underlying mechanisms of fibroblast growth factor 13 in Alzheimer's disease remain unclear. In this study, we established rat models of Alzheimer's disease by stereotaxic injection of amyloid-β ($A\beta_{1-42}$)-induced into bilateral hippocampus. We also injected lentivirus containing fibroblast growth factor 13 into bilateral hippocampus to overexpress fibroblast growth factor 13. The expression of fibroblast growth factor 13 was downregulated in the brain of the Alzheimer's disease model rats. After overexpression of fibroblast growth factor 13, learning and memory abilities of the Alzheimer's disease model rats were remarkably improved. Fibroblast growth factor 13 overexpression increased brain expression levels of oxidative stress-related markers glutathione, superoxide dismutase, phosphatidylinositol-3-kinase, AKT and glycogen synthase kinase 3β, and anti-apoptotic factor BCL. Furthermore, fibroblast growth factor 13 overexpression decreased the number of apoptotic cells, expression of pro-apoptotic factor BAX, cleaved-caspase 3 and amyloid-β expression, and levels of tau phosphorylation, malondialdehyde, reactive oxygen species and acetylcholinesterase in the brain of Alzheimer's disease model rats. The changes were reversed by the phosphatidylinositol-3-kinase inhibitor LY294002. These findings suggest that overexpression of fibroblast growth factor 13 improved neuronal damage in a rat model of Alzheimer's disease through activation of the phosphatidylinositol-3-kinase/AKT/glycogen synthase kinase 3β signaling pathway.

Key Words: AKT; Alzheimer's disease; amyloid-β; apoptosis; cognitive dysfunction; fibroblast growth factor 13; glycogen synthase kinase 3β; neuronal damage; oxidative stress; phosphatidylinositol-3-kinase

Introduction

Alzheimer's disease (AD) is a progressive neurodegenerative disease that is the most common cause of dementia, and is the sixth primary cause of death around the world (Zhang et al., 2019). AD is identified by impairments in learning, memory and cognition, as well as changes in mood (Matej et al., 2019). The two significant AD pathologies are the deposition of aggregated amyloid-β (Aβ) plaques and neurofibrillary tangles composed of hyperphosphorylated tau protein (d'Errico and Meyer-Luehmann, 2020). Aβ is produced from the amyloid precursor protein in which the β-site amyloid precursor protein cleaving enzyme 1 and γ-secretase cleave amyloid precursor protein into the Aβ peptide ($A\beta_{1-40}$ or $A\beta_{1-42}$) (Hampel et al., 2021). The amyloid cascade hypothesis states that Aβ accumulation evokes a series of pathological alterations, such as tau phosphorylation, neurofibrillary tangle formation, synaptic loss, neuronal death and cognitive deficits (Hardy and Higgins, 1992). Thus, Aβ is strongly related to the risk of Alzheimer's dementia (van Oijen et al., 2006).

Fibroblast growth factor 13 (FGF13) is an intracellular nonsecretory protein belonging to the FGF homologous factor subfamily (Goldfarb, 2005). Human FGF13 is generally distributed in human fetal and adult brain, especially in the cortex and cerebellum, and in adult kidney (Greene et al., 1998), and murine FGF13 is expressed in the embryonic nervous system, heart and connective tissue (Hartung et al., 1997). Functionally, FGF13 acts as a microtubule-stabilizing protein to modulate neuronal polarization and migration, and axonal formation and refinement (Wu et al., 2012). Similar roles of FGF13 have also been observed after spinal cord injury, and overexpression of FGF13 is necessary for axonal regeneration through the increase of mitochondrial function in primary cortical neurons (Li et al., 2018). In addition, downregulation of FGF13 impairs the excitability of inhibitory interneurons, which elevates the excitability within local hippocampal circuits and causes the clinical phenotype of epilepsy (Puranam et al., 2015). Moreover, loss of FGF13 impairs learning and memory in mice (Wu et al., 2012). More importantly, gene expression profiling results show that FGF13 is downregulated in brain of both AD patients and mice (Castillo et al., 2017). Thus, these reports indicate that FGF13 plays an important role in AD. Nevertheless, the mechanism of FGF13 in AD remains unknown.

In the present study, the role and underlying mechanism of FGF13 were investigated in AD model rats. We hope our results can lay a theoretical foundation for the development of treatments for AD and other relevant neurodegenerative diseases.

Methods

Animals

Because male animals are large and good for experimental operation (Soria Lopez et al., 2019), male animals were used in the study. Adult male Sprague-Dawley rats (12 weeks old, 410–440 g) were purchased from Hunan SJA Laboratory Animal Co., Ltd. (Changsha, China; license No. SYXK (Xiang) 2020-0019), and were adapted to standard laboratory conditions for 1 week before experiments began. Rats were provided with a standard diet and water *ad*

Department of Traditional Chinese Medicine, The Third Xiangya Hospital of Central South University, Changsha, Hunan Province, China

***Correspondence to:** Hong Zhu, PhD, yellingu@163.com.

https://orcid.org/0000-0002-4763-4591 (Hong Zhu)

How to cite this article: *Li RM, Xiao L, Zhang T, Ren D, Zhu H (2023) Overexpression of fibroblast growth factor 13 ameliorates amyloid-β-induced neuronal damage. Neural Regen Res 18(6):1347-1353.*

libitum at 40–60% relative humidity and temperature of 25 ± 2°C with a 12/12-hour light-dark cycle, and were housed six per cage (535 mm × 390 mm × 200 mm). All operations were strictly conducted based on the Guide for the Care and Use of Laboratory Animals (National Institutes of Health, 2011). All of the experiments were executed with ethical approval as determined by the Animal Ethical Committee of Central South University (approval No. XMSB-2020-0051) on March 18, 2020. Rats were randomly divided into six groups (n = 6): sham, Aβ, Aβ + LV-NC, LV-NC, Aβ + LV-FGF13, and Aβ + LV-FGF13 + LY294002 groups. The timeline of this study is shown in **Additional Figure 1**.

Sodium dodecyl sulfate-polyacrylamide gel electrophoresis

$A\beta_{1-42}$ (Cat# SCP0038, Sigma, St. Louis, MO, USA) and scrambled $A\beta_{1-42}$ (Cat# AG916, Sigma) were analyzed by sodium dodecyl sulfate-polyacrylamide gel electrophoresis. In brief, 50 μg Aβ peptides were mixed with sodium dodecyl sulfate-polyacrylamide gel electrophoresis loading buffer, 5× dithiothreitol (Solarbio, Beijing, China), boiled for 5 minutes at 100°C, and centrifuged at 13,000 × g for 3 minutes. Then, 10 μL supernatants were loaded onto gels along with protein markers and electrophoretically isolated at 110 V. Gels were stained for total protein using the Coomassie Brilliant Blue Fast Staining solution (Solarbio).

Model construction and lentivirus transfection

The AD rat model was established via stereotaxic injection of Aβ, as described in a previous study (Li et al., 2017). In brief, rats (n = 6) were exposed to 2% isoflurane (RWD Life Science, Shenzhen, China) for 5 minutes, and then fixed on a stereotaxic frame (RWD Life Science). $A\beta_{1-42}$ at a concentration of 20 μg/3 μL (Li et al., 2017) was injected into the bilateral hippocampus (3.5 mm lateral from midline, 4.3 mm posterior to the bregma, and 3.3 mm ventral to bregma (Li et al., 2017)) through a micro-syringe at a rate of 1 μL/min. Rats in the control group were stereotaxically injected with the same amount of normal saline. Subsequently, the bilateral hippocampus of AD rats was stereotaxically injected with 2 μL lentivirus-expressed FGF13 (LV-FGF13, 2 × 10^9 transducing units/mL, Genechem, Shanghai, China) to upregulate FGF13, or with negative control (NC, Genechem). In addition, to investigate the correlation between FGF13 upregulation and changes in phosphatidylinositol-3 kinase (PI3K) signaling, the PI3K inhibitor LY294002 (30 mg/kg; Cat# 9901, Cell Signaling Technology, Inc., Danvers, MA, USA) was stereotaxically injected in bilateral hippocampus in AD model rats following 2 hours of injection of 2 μL LV-FGF13. Rats were sacrificed via inhalation with isoflurane, and the brains were immediately harvested for subsequent assays.

Hematoxylin and eosin staining

To assess the role of FGF13 in the Aβ-induced cognitive alterations, brains were dissected and fixed in 4% paraformaldehyde overnight, and then dehydrated and embedded. Next, the brains were cut into slices (5 μm) and stained with hematoxylin and eosin (Solarbio). The stained slices were captured by a digital trinocular camera microscope (CX23, Olympus, Tokyo, Japan). The pathological alterations of neurons were observed to determine neuronal damage.

Nissl staining

The damage to cortical neurons was examined by Nissl staining. Briefly, the dewaxed cortical slices were stained with Nissl stain solution (methyl violet method) (Cat# G1432, Solarbio) according to the working instructions. After the slices were dehydrated, hyalinized and mounted, they were imaged under a digital trinocular camera microscope (CX23, Olympus). Neuron numbers were analyzed to assess neuronal damage.

Quantitative reverse transcription-polymerase chain reaction

To detect FGF13 mRNA expression in the cortex, total RNA of brain tissues was obtained with TRIzol reagent (TaKaRa Biotechnology Co., Ltd., Dalian, China) and reverse transcription was performed by Bio-Rad ScripTM cDNA Synthesis Kit (Bio-Rad Laboratories, Inc., Hercules, CA, USA) according to the manufacturer's instructions. Quantitative reverse transcription-polymerase chain reaction (qRT-PCR) was conducted using the Bio-Rad CFX Manager software (Bio-Rad Laboratories, Inc.). The primer sequences of FGF13 (forward primer: 5′-GGC AAT GAA CAG CGA GGG ATA CTT GTA C-3′, reverse primer: 5′-CGG ATT GCT GCT GAC GGT AGA TCA TTG ATG-3′), and β-actin (forward primer: 5′-CTC CAT CGT CCA CCG CAA ATG CTT CT-3′, reverse primer: 5′-GCT CCA ACC GAC TGC TGT CAC CTT C-3′) were synthesized by Sangon Biotech (Shanghai, China). The conditions of qRT-PCR were 5 minutes at 94°C, followed by 40 cycles between 94°C for 15 seconds and 58°C for 30 seconds, and 72°C for 30 seconds. The relative expression level of FGF13 was analyzed using the $2^{-\Delta\Delta CT}$ method (Zhao et al., 2021) and normalized to β-actin.

Western blotting

Total protein from brain tissue was isolated by a Total Protein Extraction Kit (Cat# BC3711, Solarbio) and quantified with the bicinchoninic acid protein quantification kit (ab102536, Abcam, Cambridge, UK) according to the manufacturer's instructions. Protein samples were dissolved by 12% sodium dodecyl sulfate-polyacrylamide gel electrophoresis and electrically transferred onto polyvinylidene fluoride membranes at 150 V for 4 hours. After pre-blocking with Tris-buffered saline with Triton (Sigma) containing 3% bovine serum albumin (Sangon Biotech) for 1 hour at room temperature (25°C), the membrane was treated with primary antibody (rabbit anti-FGF13, 1:3000, Cat# ab153808, RRID: AB_2890172, Abcam; rabbit anti-BAX, 1:5000, Cat# ab32503, RRID: AB_725631, Abcam; rabbit anti-BCL-2, 1:2000, Cat# ab196495, Abcam; rabbit anti-cleaved-caspase 3, 1:500, Cat# ab2302, RRID: AB_302962, Abcam; rabbit anti-phosphorylated tau (p-tau S404), 1:2000, Cat# ab92676, RRID: AB_10561457, Abcam; rabbit anti-p-tau (T181), 1:1000, Cat# ab254409, RRID: AB_2905609, Abcam; rabbit anti-p-tau (T217), 1:1000, Cat# ab192665, Abcam; rabbit anti-tau, 1:600, Cat# 10274-1-AP, RRID: AB_2139718, Proteintech, Wuhan, China; rabbit anti-acetylcholinesterase (AChE), 1:1000, Cat# ab183591, RRID: AB_2857345, Abcam; rabbit anti-p-PI3K, 1:500, Cat# ab278545, Abcam; rabbit anti-PI3K, 1:2000, Cat# ab180967, Abcam; rabbit anti-AKT, 1:500, Cat# ab8805, RRID: AB_306791, Abcam; rabbit anti-p-AKT, 1:1000, Cat# ab38449, RRID:AB_722678, Abcam; mouse anti-glycogen synthase kinase 3 beta (GSK-3β), 1:2000, ab93926, RRID: AB_10563643, Abcam; rabbit anti-p-GSK-3β, 1:1000, Cat# ab107166, RRID: AB_11143750, Abcam; rabbit polyclonal anti-β-actin, 1:5000, Cat# ab8227, RRID: AB_2305186, Abcam) overnight at 4°C. The membrane was rinsed with Tris-buffered saline three times, then incubated with horseradish peroxidase (HRP)-conjugated goat anti-rabbit IgG H&L (1: 50 000, Abcam, Cat# ab205718, RRID: AB_2819160) or HRP-conjugated goat anti-mouse IgG H&L (1:20 000, Abcam, Cat# ab205719, RRID: AB_2755049) for 1 hour at 37°C. Visualization of the bands was performed by diaminobutyric acid (Sigma) treatment for 10 minutes and terminated by washing with distilled water. The blots were quantified with the Fluor Chem FC3 system (Alpha, Protein Simple, CA, USA) and analyzed with ImageJ 16.0 (National Institutes of Health, Bethesda, MD, USA) (Schneider et al., 2012).

Immunofluorescence assay

To examine the level of FGF13 in Aβ-induced rats, rats were transcardially perfused with ice-cold 0.1 M phosphate buffered saline (PBS; pH 7.4, Solarbio) followed by ice-cold 4% buffered paraformaldehyde (Solarbio). The rats were then sacrificed, and the brains were quickly removed and immersed in 4% buffered paraformaldehyde overnight. The brain tissues were embedded with Optimum Cutting Temperature compound (SAKURA, Torrance, CA, USA) and cut into 5 μm-thick coronal sections with a Leica CM 1950 cryostat (Leica Microsystems, Wetzlar, Germany). After being air-dried at room temperature for 30 minutes, brain sections were washed with 0.1 M PBS to clear the Optimum Cutting Temperature compound. Subsequently, sections were incubated with blocking buffer (PBS including 3% bovine serum albumin) and 0.2% Triton X-100 [Solarbio]) followed by incubation with mouse monoclonal anti-FGF13 (1:1000, Abcam, Cat# ab186300) or anti-$A\beta_{1-42}$ (1:1000, Abcam, Cat# ab11132, RRID: AB_297770) at 4°C overnight. After being washed with 0.1 M PBS for 3 × 10 min , sections were incubated with goat anti-mouse IgG-AlexaFluor 647 (1:1000, Abcam, Cat# ab150115, RRID: AB_2687948) at room temperature for 1 hour. Sections were mounted with Mounting Medium, antifading with 4′,6-diamidine-2-phenylindole (Solarbio, S2110) after three rinses in 0.1 M PBS. The fluorescence intensity was analyzed by a fluorescence microscope (Olympus, IX71).

Morris water maze test

The Morris water maze test was performed in a swimming pool with a diameter of 110 cm filled with water (22 ± 2°C) to a depth of approximately 30 cm, as described in a previous study (Yan et al., 2020). The pool was partitioned into four quadrants, one of which always contained a platform in the center except for during the experiments executed on the last day. The pool was surrounded with different cues to assist rats to recognize the spatial orientation. Learning ability of rats was assessed for 4 consecutive days. Each rat was placed into the pool facing the wall and was trained to discover the platform with four trials per day. Rats were permitted to arrive at the platform within 90 seconds, and the swim path and time to find the platform were documented through a video camera. If the time that a rat took to reach the platform exceeded 90 seconds, the rat was guided to the platform manually for 10 seconds to accommodate the environment, and the latency was designated as 90 seconds. One day after the final training, the platform was dismantled and the rats performed a free exploration experiment for 90 seconds. The time spent in the target quadrant and the swim path were monitored and analyzed via a video tracking apparatus (Ethovision XT, Noldus, Wageningen, Netherlands).

Novel object recognition test

To determine the role of FGF13 in cognitive function in the AD rats, novel object recognition tests were carried out in a cube behavior box with a side length of 30 cm in a light-proof and sound-proof environment, in accordance with a previous study (Yan et al., 2020). Rats were placed in the middle of the box without any objects and were allowed to adjust for 5 minutes. On day 1, two identical objects (blue plastic cubes, 5 cm × 5 cm × 5 cm) were put into the box and rats were placed into the box equidistant from the objects to explore freely for 5 minutes. On day 2, one of the two identical objects was replaced with a black plastic cylinder with a height of 5 cm and a diameter of 5 cm, and then rats were placed into the box to explore freely for 5 minutes. The times to contact the two objects within 10 minutes were documented. Cognitive function was assessed by the recognition index, which was a comparison between the exploration time related to either the two objects (training phase) or new objects (retention phase) and the total exploration time. A distance between the rat's nose and the object within 2 cm was identified as exploratory behavior, whereas walking surrounding the object or only moving around the object was not regarded as exploratory behavior. Between each rat, the objects and bottom of the box were scrubbed with 75% alcohol to remove the odor left by the previous rat.

Terminal deoxynucleotidyl transferase deoxyuridine triphosphate nick end labeling staining

To assess the role of FGF13 in apoptosis in the AD rats, terminal deoxynucleotidyl transferase deoxyuridine triphosphate nick end labeling (TUNEL) staining was executed with the *In Situ* Cell Death Detection Kit, POD (Cat# 11684817910, Roche, Basel, Switzerland) according to the manufacturer's instructions. Frozen brain sections were incubated with Mounting Medium, antifading with 4′,6-diamidine-2-phenylindole. The TUNEL-positive cells in six random nonoverlapping fields (400×) were quantified by ImageJ. The apoptosis rate was calculated as the number of TUNEL-positive cells to total cells.

Detection of glutathione, superoxide dismutase, malondialdehyde and reactive oxygen species

The concentrations of glutathione (GSH), superoxide dismutase (SOD), malondialdehyde (MDA) and reactive oxygen species (ROS) in frozen brain tissue were measured by commercial GSH test kit (Cat# A006-2-1, Nanjing Jiancheng Bioengineering Institute, Nanjing, China), total SOD test kit (Cat# A001-1-1, Nanjing Jiancheng Bioengineering Institute), MDA test kit (Cat# A003-1-1, Nanjing Jiancheng Bioengineering Institute) and ROS assay kit (Cat# E004-1-1, Nanjing Jiancheng Bioengineering Institute), respectively, according to the manufacturer's instructions. The absorbance of wells was read at 412 nm (GSH), 532 nm (MDA) and 560 nm (SOD) using a microplate reader (Thermo Fisher Scientific, Waltham, MA, USA). The fluorescence intensity of ROS was detected with the excitation and emission wavelengths at 500 nm and 525 nm, respectively, by Thermo Scientific Fluoroskan (Thermo Fisher Scientific).

Statistical analysis

The sample size was calculated using the following formula: sample size = the sum of experimental animals in each group − the number of groups. In a previous study (Guzmán-Ruiz et al., 2021), six rats were generally used in each group, thus, we also used six rats in each group. In the present study, a total of 36 rats was prepared, and the actual sample size was 30 rats, based on the sample size = 36 − 6 = 30. No animals or data points were excluded in the analysis. The evaluators were blinded to the assignments only for the behavioral tests. Data from more than two groups were analyzed by one-way analysis of variance with Tukey's *post hoc* test, whereas data from only two groups were analyzed with the Student's *t*-test using the SPSS 22.0 package (IBM, Armonk, NY, USA). Results were presented as the mean ± standard deviation, and the differences were regarded as statistically significant when $P < 0.05$.

Results

FGF13 expression is downregulated in Aβ-induced rats

Because the biological effects of Aβ significantly differ according to its conformational state (Nortley et al., 2019), it is important to verify the aggregation state before performing stereotaxic injection. A characteristic appearance for $Aβ_{1–42}$ is a mixture of oligomers and monomers that form at 3.5–30 kDa, whereas scrambled $Aβ_{1–42}$ mainly formed monomers (**Figure 1A**). The AD rat model was then constructed through the stereotaxic injection of $Aβ_{1–42}$ into bilateral hippocampus of rats. Hematoxylin and eosin staining revealed that the neurons in hippocampal CA1 showed disorder, sparseness, obvious nuclear contraction and neuronal swelling compared with those in sham rats (**Figure 1B**), which suggested the successful establishment of the AD rat model. Additionally, Nissl staining also showed neuronal damage in cortex, as observed by the decrease of Nissl staining (**Figure 1C**). Subsequently, the level of FGF13 was detected in Aβ-induced rats. Both the transcriptional and translational levels of FGF13 were significantly decreased in Aβ-induced rats compared with these in sham rats ($P < 0.001$; **Figure 1D–F**). Moreover, immunofluorescence further confirmed the reduction of FGF13 in Aβ-induced rats (**Figure 1G**). Thus, FGF13 was downregulated in Aβ-induced rats.

FGF13 overexpression improves cognitive dysfunction in Aβ-induced rats

To investigate the role of FGF13 in the Aβ-induced rats, LV-FGF13 or LV-NC was stereotaxically injected into the bilateral hippocampus of healthy rats. The protein level of FGF13 in the cortex was notably enhanced in the Aβ + LV-FGF13 group compared with that in the LV-NC group ($P < 0.001$; **Figure 2A**). Moreover, LV-FGF13 or LV-NC was also stereotaxically injected into the bilateral hippocampus of Aβ-induced rats to upregulate the level of FGF13. Western blot showed that FGF13 overexpression significantly rescued the Aβ-induced decrease in FGF13 protein level ($P < 0.001$; **Figure 2B**), which verified the efficiency of lentivirus overexpression.

Morris water maze tests showed that FGF13 overexpression markedly reduced the escape latency compared to that in Aβ-induced rats ($P < 0.001$), which indicated that FGF13 upregulation ameliorated Aβ-induced learning deficits in Aβ-induced rats (**Figure 2C**). Additionally, Aβ-induced rats spent much less time in the target quadrant compared with that in the sham group ($P < 0.001$), and Aβ-induced rats with increased FGF13 expression spent more time in the target quadrant than did Aβ-induced rats without FGF13 overexpression ($P < 0.001$; **Figure 2D**), suggesting that FGF13 overexpression improved Aβ-induced memory defects. In the novel object recognition test, no statistical difference was observed in the recognition index of rats in the sham, Aβ, Aβ + LV-NC and Aβ + LV-FGF13 groups at day 1 ($P > 0.05$). However, the recognition index of Aβ-treated rats was greatly decreased compared with that of sham rats, which was observably reversed with FGF13 upregulation on day 2 ($P < 0.001$; **Figure 2E**). The results suggested that the increased expression of FGF13 ameliorated the recognition disorder in rats induced by Aβ. Taken together, these findings indicate that FGF13 overexpression improved the cognitive dysfunction in Aβ-induced rats.

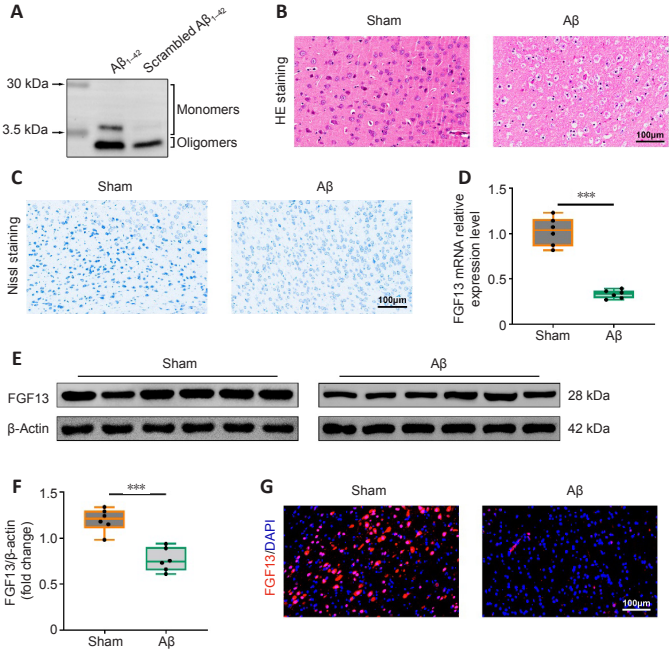

Figure 1 | FGF13 expression level is downregulated in Aβ-induced rats.

(A) The aggregation state of Aβ before performing stereotaxic injection in rats was determined by SDS-PAGE. (B) H&E staining in hippocampal CA1 of Aβ-induced rats and sham rats (400× original magnification, scale bar: 100 μm). The neurons in hippocampal CA1 of Aβ-induced rats showed disorder, sparseness, obvious nuclear contraction and neuronal swelling compared with those in sham rats. (C) Nissl staining in cortex of Aβ-induced rats and sham rats (400× original magnification, scale bar: 100 μm). Neuronal damage was observed in cortex, as shown by the decrease of Nissl staining. (D) FGF13 mRNA level was examined by qRT-PCR. The data were normalized to β-actin. (E, F) FGF13 protein level was detected by western blot. The data were normalized to β-actin. Data are expressed as mean ± SD ($n = 6$). ***$P < 0.001$ (Student's *t*-test). (G) FGF13 level (red, AlexaFluor 647) was assessed. IF confirmed the reduction of FGF13 in Aβ-induced rats. Aβ: Amyloid-β; DAPI: 4′,6-diamidine-2-phenylindole; FGF13: fibroblast growth factor 13; H&E: hematoxylin and eosin; IF: immunofluorescence; qRT-PCR: reverse transcription-quantitative polymerase chain reaction; SDS-PAGE: sodium dodecyl sulfate-polyacrylamide gel electrophoresis.

FGF13 overexpression inhibits apoptosis in the brain of Aβ-induced rats

Apoptosis in brain of Aβ-induced rats with or without overexpression of FGF13 was detected by TUNEL assay. The apoptosis rate of Aβ-induced rats was dramatically elevated compared with that of sham rats, and the rate was significantly reduced with upregulation of FGF13 ($P < 0.001$; **Figure 3A**). Furthermore, FGF13 overexpression significantly attenuated the Aβ-induced increases in the protein levels of BAX and cleaved-caspase 3, and significantly reversed the Aβ-induced decrease in the relative protein level of BCL-2 ($P < 0.001$; **Figure 3B**). Therefore, these results suggest that FGF13 overexpression suppressed apoptosis in the Aβ-induced rat brain.

FGF13 overexpression alleviates the oxidative stress response in the brain of Aβ-induced rats

We next investigated the role of FGF13 in the oxidative stress response in the brain of Aβ-induced rats. The concentrations of GSH ($P < 0.001$) and SOD ($P < 0.01$) in the brain of Aβ-induced rats were significantly decreased compared with those in brain of sham rats, and the decrease was markedly reversed with the overexpression of FGF13 ($P < 0.05$; **Figure 4A**). In contrast, FGF13 upregulation significantly reduced the MDA concentration and ROS content compared with these in Aβ-induced rats ($P < 0.001$; **Figure 4A** and **B**). Therefore, these results suggested that overexpression of FGF13 relieved the oxidative stress response in the brain of Aβ-induced rats.

FGF13 overexpression improves Aβ accumulation and hyperphosphorylated tau in the brain of Aβ-induced rats

The fluorescence intensity of Aβ in the Aβ-induced rat brain was significantly enhanced compared with that in sham rats (**Figure 5A**), which was markedly reversed by overexpression of FGF13. In addition, FGF13 upregulation decreased the Aβ-induced protein levels of p-tau (Ser 404, Thr 181 and Thr 217) and total tau ($P < 0.01$; **Figure 5B**). Similarly, FGF13 upregulation notably diminished the relative protein expression of AChE compared with these in Aβ-induced rats ($P < 0.05$; **Figure 5C**). Thus, these results suggested that FGF13 overexpression ameliorated pathological AD features.

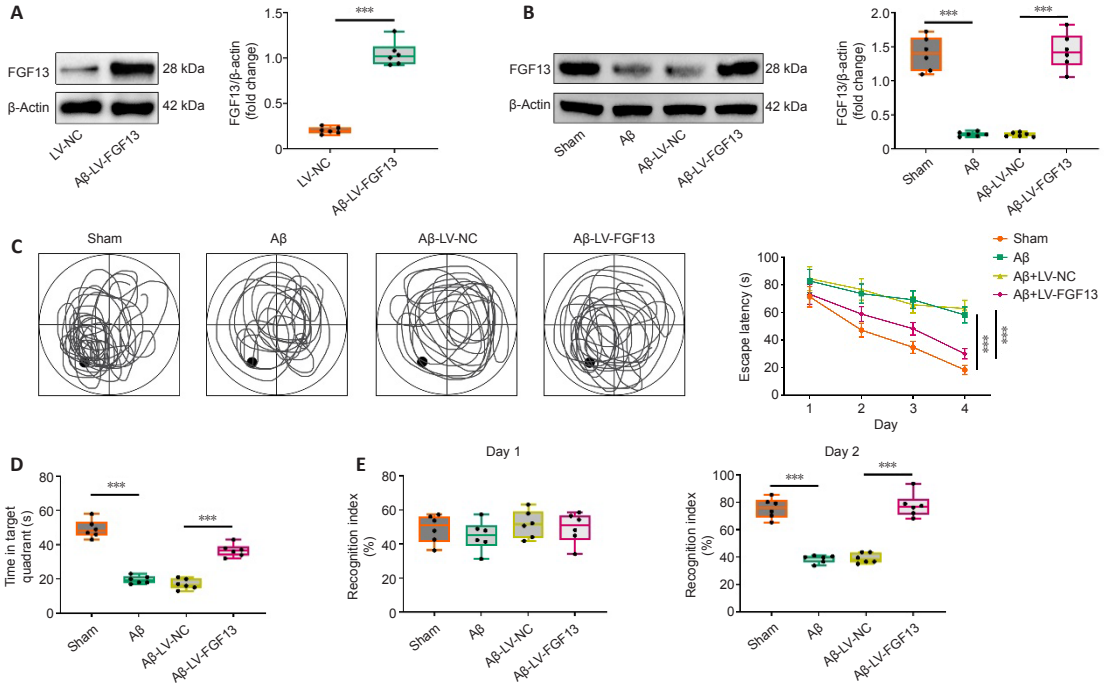

Figure 2 | **FGF13 overexpression ameliorates the cognitive dysfunction in Aβ-induced rats.**
(A, B) The protein level of FGF13 was examined by western blot. The data were normalized to β-actin. (C, D) Escape latency and time spent in the target quadrant were evaluated by Morris water maze test. FGF13 upregulation notably ameliorated Aβ-induced learning deficits in Aβ-induced rats. (E) The recognition index in novel object recognition test was assessed. Data are expressed as mean ± SD (n = 6). ***P < 0.001 (Student's t-test [A] or one-way analysis of variance followed by Tukey's *post hoc* test [B–E]). Aβ: Amyloid-β; FGF13: fibroblast growth factor 13; LV: lentivirus; NC: negative control.

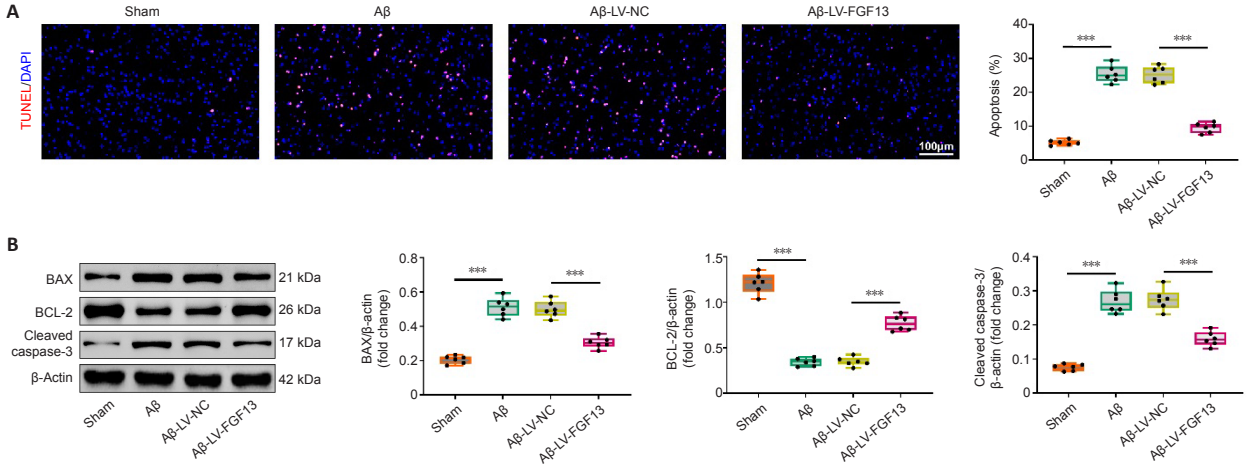

Figure 3 | **FGF13 overexpression represses neuronal apoptosis in the brain of Aβ-induced rats.**
(A) Apoptosis in brain was determined by TUNEL staining (400× original magnification, scale bar: 100 μm). FGF13 upregulation reversed the Aβ-induced change in apoptosis rate. (B) The protein levels of BAX, BCL-2 and cleaved-caspase 3 were assessed by western blot assay. The data were normalized to β-actin. Data are expressed as mean ± SD (n = 6). ***P < 0.001 (one-way analysis of variance followed by Tukey's *post hoc* test). Aβ: Amyloid β; DAPI: 4′,6-diamidine-2-phenylindole; FGF13: fibroblast growth factor 13; LV: lentivirus; NC: negative control; TUNEL: terminal deoxynucleotidyl transferase deoxyuridine triphosphate nick end labeling.

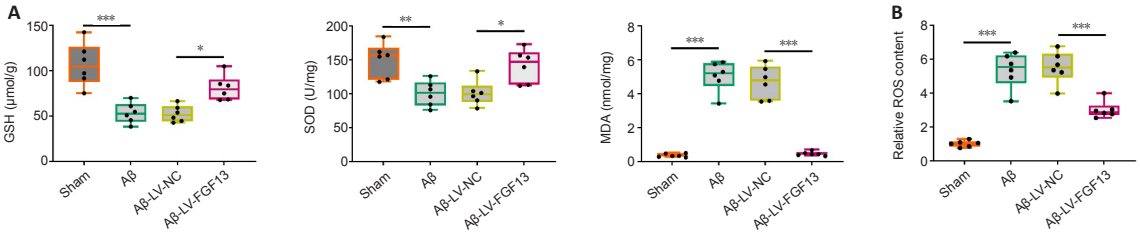

Figure 4 | **FGF13 upregulation alleviates the oxidative stress response in the brain of Aβ-induced rats.**
(A, B) GSH, SOD and MDA concentrations (A) and ROS content (B) were measured by commercial kits. Data are expressed as mean ± SD (n = 6). *P < 0.05, **P < 0.01, ***P < 0.001 (one-way analysis of variance followed by Tukey's *post hoc* test). Aβ: Amyloid β; FGF13: fibroblast growth factor 13; GSH: glutathione; LV: lentivirus; MAD: malondialdehyde; NC: negative control; ROS: reactive oxygen species; SOD: superoxide dismutase.

FGF13 overexpression ameliorates Aβ-associated neuronal damage through activating the PI3K/AKT/GSK-3β pathway

To investigate the potential molecular mechanism of FGF13 in the Aβ-induced rat brain, we used western blotting to examine the relative expression levels of proteins related to a potential signaling pathway. Expression levels of p-PI3K/PI3K, p-AKT/AKT, and p-GSK-3β/GSK-3β in the Aβ-induced rats were reduced compared with those in sham rats ($P < 0.001$), which was significantly reversed by FGF13 overexpression ($P < 0.05$; **Figure 6**). The results suggest that overexpression of FGF13 activated the PI3K/AKT/GSK-3β axis.

To investigate the direct correlation between FGF13 upregulation and changes in PI3K signaling, a PI3K inhibitor, LY294002, was applied. In the behavioral tests, LY294002 treatment significantly reduced the LV-FGF13-induced increases in time spent in the target quadrant and the recognition index on day 2 in Aβ rats ($P < 0.01$), though no statistical difference was observed in the recognition index on day 1 ($P > 0.05$; **Figure 7A** and **B**). LY294002 significantly increased the LV-FGF13-induced decreases in the protein expression of BAX and cleaved-caspase 3 in the cortex ($P < 0.01$), and the reverse effect was observed in the protein expression of BCL-2 in Aβ rats ($P < 0.01$; **Figure 7C**). Furthermore, FGF13 overexpression significantly decreased the Aβ-induced increase in ROS content in the cortex ($P < 0.001$), which was markedly reversed with LY294002 treatment ($P < 0.001$; **Figure 7D**). In addition, LY294002 also significantly reversed the LV-FGF13-induced decreases in the protein expression of p-tau (Ser 404, Thr 181 and Thr 217), total tau and AChE in the cortex in Aβ rats ($P < 0.01$; **Figure 7E** and **F**). Taken together, these data indicated that upregulation of FGF13 improved Aβ-associated neuronal damage through activating the PI3K/AKT/GSK-3β pathway.

Discussion

In the present study, the role and potential molecular mechanism of FGF13 were explored in Aβ-induced rats. The results suggest that overexpression of FGF13 improved Aβ-associated neuronal damage through activating the PI3K/AKT/GSK-3β axis.

Aβ not only accumulates in the cellular matrix but also elicits microglial activation and neuroinflammation, which play a significant role in the progress of AD (Kaur et al., 2019). Injection of Aβ oligomer into hippocampus is widely applied for the construction of AD animal models (Ji et al., 2016). Similar to the study reported by Li et al. (2017), we chose $Aβ_{1–42}$ to establish the AD rat model stereotaxically. Learning and memory function were expectedly impaired in Aβ-induced rats, as indicated by the increase in swimming escape latency and reduced time spent in the target quadrant in the Morris water maze test, and by the reduced recognition index on day two of the novel object recognition test. However, FGF13 overexpression in Aβ-induced rats significantly ameliorated their impaired learning and memory, which is consistent with a previous study (Wu et al., 2012) that reported that FGF13-deficient mice displayed impaired learning and memory. Additionally, in agreement with a study by Castillo et al. (2017), we found that the level of FGF13 was downregulated in Aβ-induced rats via qRT-PCR, western blot and immunofluorescence. Therefore, these results suggest that reducing FGF13 impaired learning and memory.

Aβ deposition can cause the production of ROS and reactive nitrogen species in the brain (Varadarajan et al., 2000), which promotes the loss of synapses and neurons, and cognitive attenuation (Agostinho et al., 2010). Thus, oxidative stress is also a recognized mechanism of AD (Agostinho et al., 2010).

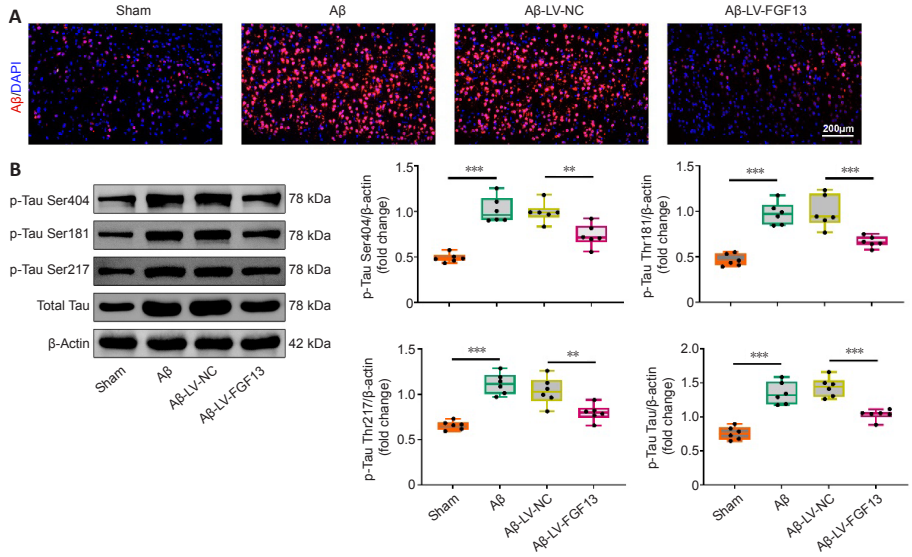

Figure 5 | **FGF13 overexpression ameliorates AD pathological characteristics.**
(A) Aβ (red: AlexaFluor 647) in the brain was examined by immunofluorescence. FGF13 overexpression markedly reversed the Aβ-induced fluorescence intensity. Scale bar: 200 μm. (B, C) Protein levels of p-tau (Ser 404, Thr 181 and Thr 217), total tau and AChE were evaluated by western blot. The data were normalized to β-actin. Data are expressed as mean ± SD ($n = 6$). *$P <$ 0.05, **$P < 0.01$, ***$P < 0.001$ (one-way analysis of variance followed by Tukey's *post hoc* test). AchE: Acetylcholinesterase; Aβ: amyloid β; DAPI: 4′,6-diamidine-2-phenylindole; FGF13: fibroblast growth factor 13; LV: lentivirus; NC: negative control; p-Tau: phosphorylated Tau; Ser: serine; Thr: threonine.

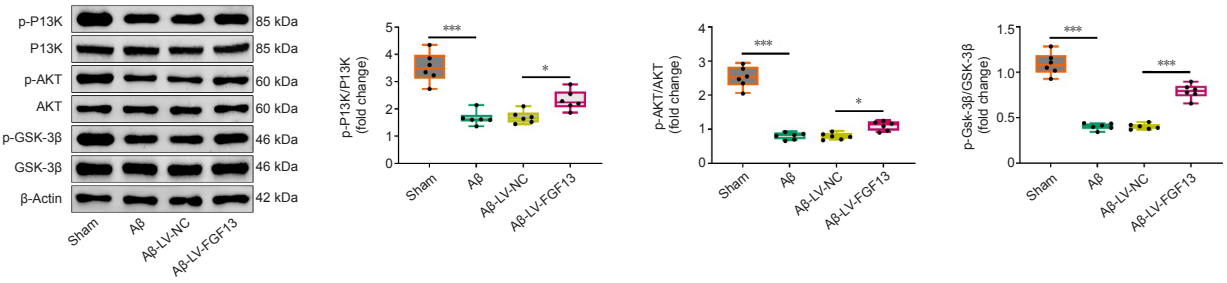

Figure 6 | **FGF13 overexpression activates the PI3K/AKT/GSK-3β pathway.**
The level of p-PI3K/PI3K, p-AKT/AKT, and p-GSK-3β/GSK-3β were measured by western blot. The data were normalized to β-actin. Data are expressed as mean ± SD ($n = 6$). *$P < 0.05$, ***$P < 0.001$ (one-way analysis of variance followed by Tukey's *post hoc* test). AKT: Protein kinase B; Aβ: amyloid β; FGF13: fibroblast growth factor 13; GSK-3β: glycogen synthase kinase 3 beta; LV: lentivirus; NC: negative control; p-AKT: phosphorylated AKT; p-GSK-3β: phosphorylated GSK-3β; PI3K: phosphatidylinositol-3 kinase; p-PI3K: phosphorylated PI3K.

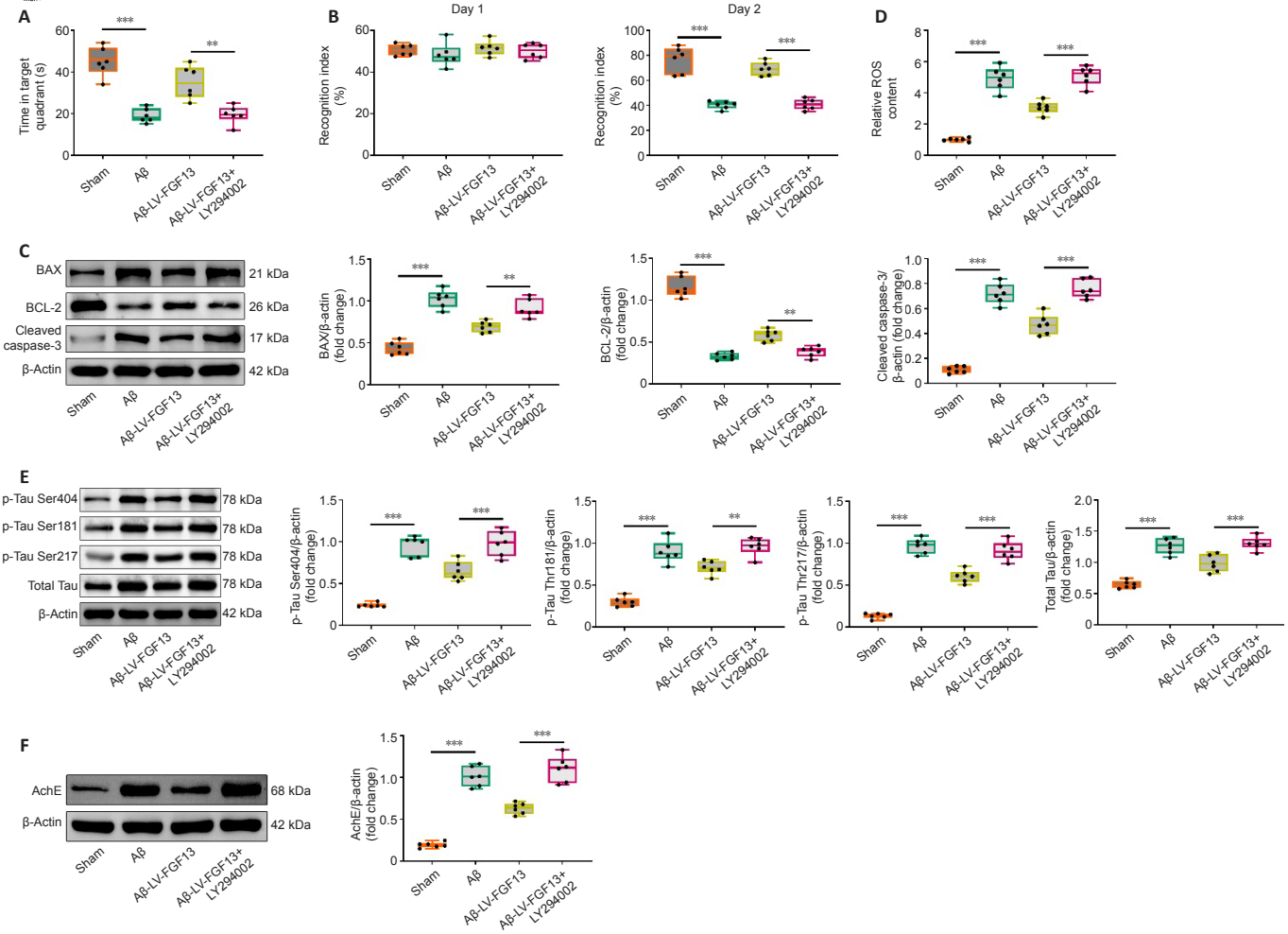

Figure 7 | **FGF13 overexpression improves Aβ-associated neuronal damage through activating the PI3K/AKT/GSK-3β pathway.**
(A, B) Time spent in the target quadrant and the recognition index of rats were evaluated by Morris water maze (A) and novel object recognition tests (B), respectively. (C) The protein levels of BAX, BCL-2 and cleaved-caspase 3 were detected by western blotting. The data were normalized to β-actin. (D) The relative ROS content was measured by a commercial kit. (E, F) The protein levels of p-tau (Ser 404, Thr 181 and Thr 217), total tau and AChE were determined by western blot. The data were normalized to β-actin. Data are expressed as mean ± SD (*n* = 6). ***P* < 0.01, ****P* < 0.001 (one-way analysis of variance followed by Tukey's *post hoc* test). AchE: Acetylcholinesterase; AKT: protein kinase B; Aβ: amyloid β; FGF13: fibroblast growth factor 13; GSK-3β: glycogen synthase kinase 3 beta; LV: lentivirus; LY294002: an inhibitor of PI3K; p-Tau: phosphorylated Tau; ROS: reactive oxygen species; Ser: serine; Thr: threonine.

In the present study, upregulation of FGF13 notably elevated the Aβ-induced decreases in GSH and SOD concentrations, and reduced the Aβ-induced increases in MDA concentration and relative ROS content in the Aβ-induced rat brain. SOD is an antioxidant enzyme that specifically scavenges oxygen free radicals. It plays a vital role in the balance of oxidation and antioxidants, and catalyzes the disproportionation of superoxide anion free radicals to generate hydrogen peroxide, which is subsequently converted into water by GSH peroxidase (Asadi et al., 2021). MDA is a degradation product of lipid peroxides that represents the peroxidation degree of body fat (Askari et al., 2021). As the major free radical in the body, ROS is not only oxidizing, but also can trigger a cascade reaction, thereby generating more ROS (Schieber and Chandel, 2014). Overabundance of ROS is the dominating precursor of oxidative stress (Schieber and Chandel, 2014). Thus, our results indicated that FGF13 overexpression dampened the Aβ-facilitated oxidative stress response. Additionally, neuronal oxidative stress elicited by Aβ deposition leads to neuronal death through the stimulation of apoptotic signaling (Tamagno et al., 2003). The anti-apoptosis factor Bcl-2 and pro-apoptosis factor BAX modulate the progress of apoptosis (Edlich, 2018), and cleaved-caspase 3, an active form of caspase 3, regulates the different phases in the apoptotic pathway (Asadi et al., 2021). Our results showed that the apoptosis rate, and the relative protein levels of BAX and cleaved-caspase 3 were dramatically elevated, and the relative protein level of BCL-2 was decreased in Aβ-induced rats, which is in line with the report that Aβ suppresses Bcl-2 and accelerates BAX (Tortosa et al., 1998). However, FGF13 overexpression significantly reversed the Aβ-induced apoptotic changes, which suggests that upregulation of FGF13 attenuates Aβ-induced cell apoptosis. In brief, these findings suggest that FGF13 overexpression might improve the impaired learning and memory induced by Aβ via reducing the oxidative stress response and cell apoptosis.

The amyloid hypothesis and cholinergic hypothesis are the two main AD hypotheses (Breijyeh and Karaman, 2020). Aβ facilitates the phosphorylation of tau, and in turn, tau modulates Aβ toxicity (Zhang et al., 2021). Thus, Aβ deposition induces the generation of tau pathology and neurotoxicity, which results in neuronal death and neurodegeneration (Breijyeh and Karaman, 2020). Barthélemy et al. (2020) reported that p-tau-217 and p-tau-181 were highly specific for amyloid plaque pathology in cerebrospinal fluid. Additionally, AChE is the primary hydrolyzing enzyme of the cholinergic system that mediates neuronal survival and function (Halliday and Greenfield, 2012). Therefore, several approaches, including anticholinesterase inhibitors, beta-secretase inhibitors and anti-tau, are the most crucial therapeutic targets in AD (Ahmed et al., 2021). In the present study, the expression levels of Aβ, p-tau (Ser 404, Thr 181 and Thr 217) and AChE were significantly increased in the Aβ-induced rat brain, which were significantly reversed by the upregulation of FGF13. Hence, overexpression of FGF13 might relieve the primary pathological features of Aβ-induced rats.

The PI3K/AKT signaling pathway is one of the most important and common pathways involved in AD (Razani et al., 2021). The PI3K/AKT signaling pathway has been demonstrated to inactivate downstream GSK-3β via phosphoinositide Akt phosphorylation at serine 9 (Danielsen et al., 2015). GSK-3β is a core kinase for pathological tau hyperphosphorylation, and its inactivation can result in Aβ deposits (Mazanetz and Fischer, 2007). Thus, the PI3K/AKT/GSK-3β signaling axis plays an important role in the progress of AD. It has been shown that natural dietary supplementation of anthocyanins alleviates oxidative stress, impaired memory and neurodegeneration in an AD mouse model through the PI3K/AKT/GSK-3β axis (Ali et al., 2018). Bis(ethylmaltolato)oxidovanadium(iv) decreases tau hyperphosphorylation via activating the PI3K/Akt/GSK-3β pathway (He et al., 2020). Furthermore, β- or γ-secretase-regulated proteolytic course of amyloid precursor protein in platelet may occur via the PI3K/Akt/GSK-3β signaling pathway (Chen et al., 2019). Our results showed that FGF13 upregulation notably reversed the Aβ-induced reduction of the ratio of p-PI3K and PI3K, p-AKT and AKT, and p-GSK-3β and GSK-3β. Moreover, the ameliorative role of FGF13 overexpression in Aβ-associated neuronal damage was blocked with the application of the PI3K inhibitor LY294002. Thus, the results suggest that effect of FGF13 upregulation in Aβ-induced rats was mediated by via the PI3K/AKT/GSK-3β pathway.

Several limitations should be addressed in future studies. Although viral rescue has been demonstrated to ameliorate Aβ-associated neuronal damage, a knock-in verification may provide more reliable results. Additionally, the results should be validated in a commercial AD model. In conclusion, the findings suggested that the expression level of FGF13 was downregulated in Aβ-induced rats, which led to learning and memory deficits, increased cell apoptosis and oxidative stress response, pathological features, and reduced activation of the PI3K/AKT/GSK-3β pathway. Therefore, we concluded that overexpression of FGF13 improved Aβ-associated neuronal damage by activating the PI3K/AKT/GSK-3β axis. We hope the findings provide evidence for a potential avenue to investigate in the development of therapeutics for AD and other related neurodegenerative diseases.

Author contributions: *Conceptualization, methodology, software, data curation: RML, HZ; writing-original draft preparation, visualization, investigation, supervision: TZ, DR; validation, writing-reviewing and editing: LX. All authors approved the final version of the manuscript.*
Conflicts of interest: *The authors declare that there is no conflict of interests.*
Availability of data and materials: *All data generated or analyzed during this study are included in this published article and its supplementary information files.*

Additional file:
Additional Figure 1: *Timeline diagram in this study.*

References

Agostinho P, Cunha RA, Oliveira C (2010) Neuroinflammation, oxidative stress and the pathogenesis of Alzheimer's disease. Curr Pharm Des 16:2766-2778.
Ahmed S, Khan ST, Zargaham MK, Khan AU, Khan S, Hussain A, Uddin J, Khan A, Al-Harrasi A (2021) Potential therapeutic natural products against Alzheimer's disease with Reference of Acetylcholinesterase. Biomed Pharmacother 139:111609.
Ali T, Kim T, Rehman SU, Khan MS, Amin FU, Khan M, Ikram M, Kim MO (2018) Natural dietary supplementation of anthocyanins via PI3K/Akt/Nrf2/HO-1 pathways mitigate oxidative stress, neurodegeneration, and memory impairment in a mouse model of Alzheimer's disease. Mol Neurobiol 55:6076-6093.
Asadi M, Taghizadeh S, Kaviani E, Vakili O, Taheri-Anganeh M, Tahamtan M, Savardashtaki A (2021) Caspase-3: Structure, function, and biotechnological aspects. Biotechnol Appl Biochem doi: 10.1002/bab.2233.
Askari M, Mozaffari H, Darooghegi Mofrad M, Jafari A, Surkan PJ, Amini MR, Azadbakht L (2021) Effects of garlic supplementation on oxidative stress and antioxidative capacity biomarkers: A systematic review and meta-analysis of randomized controlled trials. Phytother Res 35:3032-3045.
Barthélemy NR, Horie K, Sato C, Bateman RJ (2020) Blood plasma phosphorylated-tau isoforms track CNS change in Alzheimer's disease. J Exp Med 217:e20200861.
Breijyeh Z, Karaman R (2020) Comprehensive review on Alzheimer's disease: causes and treatment. Molecules 25:5789.
Castillo E, Leon J, Mazzei G, Abolhassani N, Haruyama N, Saito T, Saido T, Hokama M, Iwaki T, Ohara T, Ninomiya T, Kiyohara Y, Sakumi K, LaFerla FM, Nakabeppu Y (2017) Comparative profiling of cortical gene expression in Alzheimer's disease patients and mouse models demonstrates a link between amyloidosis and neuroinflammation. Sci Rep 7:17762.
Chen L, Xu S, Wu T, Shao Y, Luo L, Zhou L, Ou S, Tang H, Huang W, Guo K, Xu J (2019) Abnormal platelet amyloid-β precursor protein metabolism in SAMP8 mice: Evidence for peripheral marker in Alzheimer's disease. J Cell Physiol 234:23528-23536.
d'Errico P, Meyer-Luehmann M (2020) Mechanisms of pathogenic Tau and Aβ protein spreading in Alzheimer's disease. Front Aging Neurosci 12:265.
Danielsen SA, Eide PW, Nesbakken A, Guren T, Leithe E, Lothe RA (2015) Portrait of the PI3K/AKT pathway in colorectal cancer. Biochim Biophys Acta 1855:104-121.
Edlich F (2018) BCL-2 proteins and apoptosis: recent insights and unknowns. Biochem Biophys Res Commun 500:26-34.
Goldfarb M (2005) Fibroblast growth factor homologous factors: evolution, structure, and function. Cytokine Growth Factor Rev 16:215-220.
Greene JM, Li YL, Yourey PA, Gruber J, Carter KC, Shell BK, Dillon PA, Florence C, Duan DR, Blunt A, Ornitz DM, Ruben SM, Alderson RF (1998) Identification and characterization of a novel member of the fibroblast growth factor family. Eur J Neurosci 10:1911-1925.
Guzmán-Ruiz MA, Herrera-González A, Jiménez A, Candelas-Juárez A, Quiroga-Lozano C, Castillo-Díaz C, Orta-Salazar E, Organista-Juárez D, Díaz-Cintra S, Guevara-Guzmán R (2021) Protective effects of intracerebroventricular adiponectin against olfactory impairments in an amyloid β(1-42) rat model. BMC Neurosci 22:14.
Halliday AC, Greenfield SA (2012) From protein to peptides: a spectrum of non-hydrolytic functions of acetylcholinesterase. Protein Pept Lett 19:165-172.
Hampel H, Vassar R, De Strooper B, Hardy J, Willem M, Singh N, Zhou J, Yan R, Vanmechelen E, De Vos A, Nisticò R, Corbo M, Imbimbo BP, Streffer J, Voytyuk I, Timmers M, Tahami Monfared AA, Irizarry M, Albala B, Koyama A, et al. (2021) The β-secretase BACE1 in Alzheimer's disease. Biol Psychiatry 89:745-756.
Hardy JA, Higgins GA (1992) Alzheimer's disease: the amyloid cascade hypothesis. Science 256:184-185.
Hartung H, Feldman B, Lovec H, Coulier F, Birnbaum D, Goldfarb M (1997) Murine FGF-12 and FGF-13: expression in embryonic nervous system, connective tissue and heart. Mech Dev 64:31-39.
He Z, Han S, Wu C, Liu L, Zhu H, Liu A, Lu Q, Huang J, Du X, Li N, Xie Q, Wan L, Ni J, Chen L, Yang X, Liu Q (2020) Bis(ethylmaltolato)oxidovanadium(iv) inhibited the pathogenesis of Alzheimer's disease in triple transgenic model mice. Metallomics 12:474-490.
Ji L, Zhao X, Lu W, Zhang Q, Hua Z (2016) Intracellular Aβ and its pathological role in Alzheimer's disease: lessons from cellular to animal models. Curr Alzheimer Res 13:621-630.
Jia J, Wei C, Chen S, Li F, Tang Y, Qin W, Zhao L, Jin H, Xu H, Wang F, Zhou A, Zuo X, Wu L, Han Y, Han Y, Huang L, Wang Q, Li D, Chu C, Shi L, et al. (2018) The cost of Alzheimer's disease in China and re-estimation of costs worldwide. Alzheimers Dement 14:483-491.
Kaur D, Sharma V, Deshmukh R (2019) Activation of microglia and astrocytes: a roadway to neuroinflammation and Alzheimer's disease. Inflammopharmacology 27:663-677.
Li J, Wang Q, Wang H, Wu Y, Yin J, Chen J, Zheng Z, Jiang T, Xie L, Wu F, Zhang H, Li X, Xu H, Xiao J (2018) Lentivirus mediating FGF13 enhances axon regeneration after spinal cord injury by stabilizing microtubule and improving mitochondrial function. J Neurotrauma 35:548-559.
Li Q, Cui J, Fang C, Liu M, Min G, Li L (2017) S-adenosylmethionine attenuates oxidative stress and neuroinflammation induced by amyloid-β through modulation of glutathione metabolism. J Alzheimers Dis 58:549-558.
Matej R, Tesar A, Rusina R (2019) Alzheimer's disease and other neurodegenerative dementias in comorbidity: A clinical and neuropathological overview. Clin Biochem 73:26-31.
Mazanetz MP, Fischer PM (2007) Untangling tau hyperphosphorylation in drug design for neurodegenerative diseases. Nat Rev Drug Discov 6:464-479.
National Institutes of Health (2011) Guide for the Care and Use of Laboratory Animals, 8th ed. Washington, DC, USA: National Academies Press.
Nortley R, Korte N, Izquierdo P, Hirunpattarasilp C, Mishra A, Jaunmuktane Z, Kyrargyri V, Pfeiffer T, Khennouf L, Madry C, Gong H, Richard-Loendt A, Huang W, Saito T, Saido TC, Brandner S, Sethi H, Attwell D (2019) Amyloid β oligomers constrict human capillaries in Alzheimer's disease via signaling to pericytes. Science 365:eaav9518.
Puranam RS, He XP, Yao L, Le T, Jang W, Rehder CW, Lewis DV, McNamara JO (2015) Disruption of Fgf13 causes synaptic excitatory-inhibitory imbalance and genetic epilepsy and febrile seizures plus. J Neurosci 35:8866-8881.
Razani E, Pourbagheri-Sigaroodi A, Safaroghli-Azar A, Zoghi A, Shanaki-Bavarsad M, Bashash D (2021) The PI3K/Akt signaling axis in Alzheimer's disease: a valuable target to stimulate or suppress? Cell Stress Chaperones 26:871-887.
Schieber M, Chandel NS (2014) ROS function in redox signaling and oxidative stress. Curr Biol 24:R453-462.
Schneider CA, Rasband WS, Eliceiri KW (2012) NIH Image to ImageJ: 25 years of image analysis. Nat Methods 9:671-675.
Soria Lopez JA, González HM, Léger GC (2019) Alzheimer's disease. Handb Clin Neurol 167:231-255.
Tamagno E, Parola M, Guglielmotto M, Santoro G, Bardini P, Marra L, Tabaton M, Danni O (2003) Multiple signaling events in amyloid beta-induced, oxidative stress-dependent neuronal apoptosis. Free Radic Biol Med 35:45-58.
Tortosa A, López E, Ferrer I (1998) Bcl-2 and Bax protein expression in Alzheimer's disease. Acta Neuropathol 95:407-412.
van Oijen M, Hofman A, Soares HD, Koudstaal PJ, Breteler MM (2006) Plasma Abeta(1-40) and Abeta(1-42) and the risk of dementia: a prospective case-cohort study. Lancet Neurol 5:655-660.
Varadarajan S, Yatin S, Aksenova M, Butterfield DA (2000) Review: Alzheimer's amyloid beta-peptide-associated free radical oxidative stress and neurotoxicity. J Struct Biol 130:184-208.
Wu QF, Yang L, Li S, Wang Q, Yuan XB, Gao X, Bao L, Zhang X (2012) Fibroblast growth factor 13 is a microtubule-stabilizing protein regulating neuronal polarization and migration. Cell 149:1549-1564.
Yan S, Xuan Z, Yang M, Wang C, Tao T, Wang Q, Cui W (2020) CSB6B prevents β-amyloid-associated neuroinflammation and cognitive impairments via inhibiting NF-κB and NLRP3 in microglia cells. Int Immunopharmacol 81:106263.
Zhang DF, Xu M, Bi R, Yao YG (2019) Genetic analyses of Alzheimer's disease in China: achievements and perspectives. ACS Chem Neurosci 10:890-901.
Zhang H, Wei W, Zhao M, Ma L, Jiang X, Pei H, Cao Y, Li H (2021) Interaction between Aβ and Tau in the Pathogenesis of Alzheimer's Disease. Int J Biol Sci 17:2181-2192.
Zhao F, Maren NA, Kosentka PZ, Liao YY, Lu H, Duduit JR, Huang D, Ashrafi H, Zhao T, Huerta AI, Ranney TG, Liu W (2021) An optimized protocol for stepwise optimization of real-time RT-PCR analysis. Hortic Res 8:179.

C-Editor: Zhao M; S-Editors: Yu J, Li CH; L-Editors: McCollum L, Yu J, Song LP; T-Editor: Jia Y

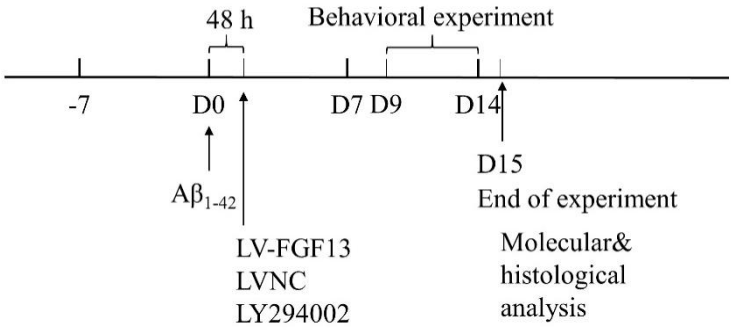

Additional Figure 1 Timeline diagram in this study.

Aβ: Amyloid β; FGF13: fibroblast growth factor 13; LV: lentivirus; LY294002: an inhibitor of phosphatidylinositol-3 kinase; NC: negative control.